

Photon-Conditioned Squeezed States for Directional Displacement Response in Continuous-Variable Photonics

Boris Kiefer^{1,*} and Olivier Pfister^{2,3}

¹*Department of Physics, New Mexico State University, Las Cruces, NM, USA*

²*Department of Physics, The University of Virginia, Charlottesville, VA, USA*

³*Charles L. Brown Department of Electrical and Computer Engineering, University of Virginia, 351 McCormick Road, Charlottesville, VA 22903, USA*

(Dated: May 28, 2026)

arXiv:2605.27660v1 [quant-ph] 26 May 2026

Abstract

Squeezed Fock states, photon-subtracted squeezed states, and optical cat states are established non-Gaussian resources in continuous-variable quantum optics. Here we compare these known state families from a task-oriented perspective: matched mean photon number, scalar Wigner negativity, and directional displacement-fidelity response. Starting from squeezed vacuum, single-photon subtraction prepares a state proportional to $S(r, \theta) |1\rangle$, while two-photon subtraction prepares an even-parity squeezed Fock superposition rather than a pure $S(r, \theta) |2\rangle$. We benchmark photon-conditioned squeezed states against Fock and coherent-cat references using the integrated Wigner negativity δ , the energy-normalized metric $\delta/\langle n \rangle$, and fidelity-threshold displacement radii $R_F(\phi)$. Cat benchmarks remain strong scalar Wigner-negativity resources, whereas photon-conditioned squeezed states provide an origin-centered alternative with tunable anisotropic displacement response. In particular, the two-photon-subtracted squeezed state shows favorable displacement-fidelity radii over selected quadrature directions at matched $\langle n \rangle$. These results identify a regime relevant to homodyne-aligned continuous-variable control and anisotropic displacement-noise mitigation, with directional sensing as a natural dual application.

I. INTRODUCTION

Non-Gaussian optical states are essential resources for continuous-variable (CV) quantum information processing. Gaussian states and Gaussian operations alone admit efficient classical descriptions, while Wigner-function negativity provides a widely used diagnostic of genuinely non-Gaussian structure and a useful resource diagnostic for CV photonics [1–5].

Squeezed number states, displaced squeezed number states, photon-subtracted squeezed states, squeezed-Fock generation protocols, and optical Schrödinger-cat states have all been studied extensively [6–17]. Recently squeezed-Fock and conditionally squeezed states have been proposed directly as bosonic-code resources [18, 19]. The purpose of the present work is therefore not to introduce a new state family, a new squeezed-Fock generation protocol, or a new bosonic code. Rather, we use photon-conditioned squeezed states as benchmarked resources and address how their matched-energy scalar and directional displacement metrics compare with Fock and cat references.

* bkiefer@nmsu.edu

The specific gap addressed here is the absence of a common matched-energy resource map that treats these established families on the same footing. Such a map separates scalar Wigner negativity from directional displacement response and clarifies how the same photon budget is distributed between non-Gaussian excitation and Gaussian squeezing. Our approach provides a common matched- $\langle n \rangle$ baseline before platform-specific costs are included.

Squeezed light provides a natural parent resource for this setting. A squeezed vacuum $S(r, \theta) |0\rangle$ is Gaussian and Wigner-positive, but conditional photon subtraction converts it into a non-Gaussian state. In the weak-tap limit, a heralding event implements the annihilation operator on the transmitted mode. A single subtraction from squeezed vacuum prepares, up to normalization and phase, the squeezed single-photon state $S(r, \theta) |1\rangle$. Higher-order subtraction produces parity-restricted squeezed Fock superpositions. In particular, two-photon subtraction does not generically prepare a pure $S(r, \theta) |2\rangle$ state. This distinction is important for connecting ideal squeezed-Fock targets with experimentally produced photon-conditioned states.

We develop a matched-mean-photon-number resource map for the sequence

$$S(r) |0\rangle, \quad aS(r) |0\rangle, \quad a^2S(r) |0\rangle, \quad (1)$$

and compare these states with Fock and coherent-cat benchmarks. The common resource budget is

$$\langle n \rangle = \langle a^\dagger a \rangle, \quad (2)$$

which fixes the excitation energy above the vacuum for a single optical mode. We evaluate both scalar Wigner metrics, negativity, δ , and negativity/photon, $\delta/\langle n \rangle$, and directional displacement fidelity metrics based on

$$F_\psi(\alpha) = |\langle \psi | D(\alpha) | \psi \rangle|^2. \quad (3)$$

The main result is a metric-dependent resource ordering. Scalar Wigner negativity and directional displacement-fidelity response do not rank the state families in the same order. Cat benchmarks can remain favorable under scalar negativity measures, while photon-conditioned squeezed states can be favorable under directional displacement-response measures when the noise or measurement axis is known. This metric-dependent ordering is the central identified resource tradeoff.

The paper is organized as follows. Section II establishes the state definitions, photon-subtraction identities, and displacement-fidelity scaling. Section III describes the matched- $\langle n \rangle$ benchmarking procedure. Section IV presents the state landscape, scalar Wigner metrics, and directional displacement-fidelity radii. Section V discusses the implications for homodyne-aligned displacement-noise mitigation and sensing.

II. THEORY

A. Conventions

We use

$$[a, a^\dagger] = 1, \quad x = \frac{a + a^\dagger}{\sqrt{2}}, \quad p = \frac{a - a^\dagger}{i\sqrt{2}}, \quad (4)$$

so that $[x, p] = i$. The Wigner function is normalized as

$$\int_{\mathbb{R}^2} W_\rho(x, p) dx dp = 1. \quad (5)$$

At the origin it is fixed by photon-number parity,

$$W_\rho(0, 0) = \frac{1}{\pi} \text{Tr}[\Pi\rho], \quad \Pi = (-1)^{a^\dagger a}. \quad (6)$$

Thus

$$W_{|n\rangle}(0, 0) = \frac{(-1)^n}{\pi}. \quad (7)$$

This provides a direct parity diagnostic for the states shown in Fig. 1.

The single-mode squeezing operator is

$$S(r, \theta) = \exp\left[\frac{1}{2}(re^{-i\theta}a^2 - re^{i\theta}a^{\dagger 2})\right]. \quad (8)$$

Unless otherwise stated, the numerical examples use real squeezing, $\theta = 0$. Squeezing in decibels is related to r by

$$r = \frac{\ln 10}{20} r_{\text{dB}}. \quad (9)$$

B. Benchmark state families

The Fock state is

$$|n\rangle = \frac{(a^\dagger)^n}{\sqrt{n!}} |0\rangle, \quad (10)$$

and a coherent state is

$$|\alpha\rangle = D(\alpha)|0\rangle, \quad D(\alpha) = \exp(\alpha a^\dagger - \alpha^* a). \quad (11)$$

Coherent states are Gaussian and Wigner-positive; in this work they enter only as components of cat-state benchmarks.

The even and odd cat states are

$$|\mathcal{C}_\pm(\alpha)\rangle = \mathcal{N}_\pm (|\alpha\rangle \pm |-\alpha\rangle). \quad (12)$$

Their mean photon numbers are

$$\langle n \rangle_{\mathcal{C}_-} = |\alpha|^2 \coth |\alpha|^2, \quad \langle n \rangle_{\mathcal{C}_+} = |\alpha|^2 \tanh |\alpha|^2. \quad (13)$$

At large $|\alpha|$, the coherent components become nearly orthogonal because

$$\langle \alpha | -\alpha \rangle = e^{-2|\alpha|^2}. \quad (14)$$

Consequently, even and odd cats become nearly degenerate in several displacement-response metrics at sufficiently large matched energy.

For squeezed Fock states,

$$|\psi_n(r, \theta)\rangle = S(r, \theta) |n\rangle, \quad (15)$$

the mean photon number is

$$\langle n \rangle_{S|n} = n + (2n + 1) \sinh^2 r. \quad (16)$$

In particular,

$$\langle n \rangle_{S|0} = \sinh^2 r, \quad \langle n \rangle_{S|1} = 1 + 3 \sinh^2 r. \quad (17)$$

C. Photon subtraction from squeezed vacuum

Photon subtraction is modeled by the action of a on the squeezed state, as realized approximately by a weak tap and conditional heralding event. Using the Bogoliubov transform we obtain

$$\begin{aligned} S^\dagger(r, \theta) a S(r, \theta) &= \mu a + \nu a^\dagger, \\ \mu &= \cosh r, \quad \nu = -e^{i\theta} \sinh r. \end{aligned} \quad (18)$$

and

$$\begin{aligned} aS(r, \theta) |0\rangle &= S(r, \theta) (\mu a + \nu a^\dagger) |0\rangle \\ &= \nu S(r, \theta) |1\rangle. \end{aligned} \tag{19}$$

Thus the normalized one-photon-subtracted squeezed vacuum is exactly a squeezed single-photon state, up to an overall phase.

For two-photon subtraction,

$$\begin{aligned} a^2 S(r, \theta) |0\rangle &= S(r, \theta) (\mu a + \nu a^\dagger)^2 |0\rangle \\ &= S(r, \theta) (\mu\nu |0\rangle + \sqrt{2}\nu^2 |2\rangle). \end{aligned} \tag{20}$$

The two-click state is therefore an even-parity squeezed superposition, not a pure $S(r, \theta) |2\rangle$ state. The relative amplitude of the $|2\rangle$ and $|0\rangle$ components in the squeezed frame is

$$\frac{\sqrt{2}\nu^2}{\mu\nu} = \sqrt{2}\frac{\nu}{\mu} = -\sqrt{2}e^{i\theta} \tanh r. \tag{21}$$

Thus, in the large-squeezing limit, the normalized state in the squeezed frame approaches an even superposition proportional to

$$|0\rangle - \sqrt{2}e^{i\theta} |2\rangle, \tag{22}$$

rather than a pure two-photon state. This provides a useful analytic reference for the numerical resource curves.

D. Scalar Wigner negativity

We quantify Wigner negativity, δ , using

$$\delta = \frac{1}{2} \left[\int_{\mathbb{R}^2} |W(x, p)| dx dp - 1 \right]. \tag{23}$$

For ideal Gaussian unitary transformations, including squeezing and phase rotations, δ is invariant under the corresponding symplectic coordinate transformation. Squeezing therefore does not create additional integrated Wigner negativity. Instead, it redistributes existing non-Gaussian structure in phase space. This observation is important for interpreting the comparison with cat states: a squeezed single-photon state can have the same δ as $|1\rangle$ while exhibiting a very different directional displacement response.

E. Displacement-fidelity radius

For a pure state $|\psi\rangle$, we define the displacement fidelity

$$F_\psi(\alpha) = |\langle\psi|D(\alpha)|\psi\rangle|^2. \quad (24)$$

This overlap is the squared magnitude of the symmetrically ordered characteristic function evaluated at the displacement amplitude. Up to the usual convention-dependent scaling of the complex phase-space argument, it is the same object that appears in displaced-number-state and displaced-squeezed-number-state overlap formulas. It therefore directly probes how distinguishable the displaced state $D(\alpha)|\psi\rangle$ is from the original state $|\psi\rangle$. In the present work we use this quantity in two complementary ways. A slowly decaying fidelity indicates robustness against displacement noise, whereas a rapidly decaying fidelity indicates sensitivity to weak displacement signals. In the numerical results, ϵ denotes the complex displacement amplitude in $D(\epsilon e^{i\phi})$, not the physical quadrature translation distance. For a displacement direction ϕ , the fidelity-threshold radius is

$$R_F(\phi) = \max \{ \epsilon : F_\psi(\epsilon e^{i\phi}) \geq F_{\text{th}} \}. \quad (25)$$

This is not a quantum-error-correction distance; no recovery map is assumed. It is a direct displacement-response diagnostic. Larger R_F means the state remains close to itself under a larger coherent displacement in that direction.

For small displacements, the fidelity has a variance-controlled expansion. A real displacement $D(\epsilon)$ translates the state along one phase-space quadrature and is generated by the conjugate quadrature; an imaginary displacement $D(i\epsilon)$ translates along the orthogonal quadrature. Thus

$$1 - F_x(\epsilon) = A \text{Var}(p) \epsilon^2 + O(\epsilon^4), \quad (26)$$

$$1 - F_p(\epsilon) = A \text{Var}(x) \epsilon^2 + O(\epsilon^4), \quad (27)$$

The proportionality constant A depends on whether ϵ denotes the complex displacement amplitude α or the corresponding quadrature translation.

The important point is independent of this convention: the two leading slopes are controlled by the conjugate quadrature variances. In the numerical implementation, we verify this relation by fitting $1 - F$ versus ϵ^2 at small ϵ and comparing the fitted slopes with the corresponding quadrature variances.

For a squeezed Fock state $S(r) |n\rangle$, the quadrature variances scale as

$$\text{Var}(x) \propto \left(n + \frac{1}{2}\right) e^{-2r}, \quad \text{Var}(p) \propto \left(n + \frac{1}{2}\right) e^{+2r}, \quad (28)$$

up to the sign convention for the squeeze axis. Therefore squeezing redistributes displacement response between conjugate quadratures. The corresponding threshold radii scale approximately as

$$R_x \sim e^{-r}, \quad R_p \sim e^{+r}, \quad (29)$$

again up to convention and state-dependent constants. This analytic scaling is the basis for interpreting the directional-radius results below.

III. NUMERICAL METHODS

All comparisons are performed at matched mean photon number $\langle n \rangle$. For each target value of $\langle n \rangle$, we solve for the squeezing r or cat amplitude α required to match that target using Eqs. (13) and (16).

The numerical parameters were kept fixed across state families within each comparison. The baseline calculations used a Fock-space cutoff of 80 and a uniform phase-space grid with 201 points along each quadrature direction over the range $x, p \in [-7, 7]$. Numerical convergence was checked by repeating the calculation with an increased Fock cutoff, an increased phase-space grid density, and an enlarged phase-space window. Across these tests, the scalar Wigner metrics changed by less than 6×10^{-3} in δ and 2×10^{-3} in $\delta/\langle n \rangle$. The displacement-fidelity radii were unchanged within numerical interpolation precision, and the ordering of state families was unchanged. These checks indicate that the reported trends are numerical features of the matched-state resource map rather than artifacts of the chosen cutoff, grid density, or phase-space window.

The squeezing was constrained to $r_{\text{dB}} \leq 12.5$, corresponding to $r \leq (\ln 10/20)12.5$, to remain within a near-term experimentally relevant squeezing range. For the cat benchmarks, the defining real α values were obtained by matching the same mean photon-number budget as the photon-conditioned squeezed states.

Unless otherwise stated, we use $F_{\text{th}} = 0.90$ across all state families, so that differences in R_x , R_p , and $R_{\text{max}}/R_{\text{min}}$ reflect state response rather than a change in the fidelity criterion.

The scalar comparison uses δ and $\delta/\langle n \rangle$. The directional comparison uses the threshold radii $R_x = R_F(0)$, $R_p = R_F(\pi/2)$, and the anisotropy ratio

$$\frac{R_{\max}}{R_{\min}} = \frac{\max_{\phi} R_F(\phi)}{\min_{\phi} R_F(\phi)}. \quad (30)$$

In the main text, R_x and R_p are evaluated along the laboratory quadrature axes. Changing the squeezing phase rotates the radius contour; therefore the physically relevant angle is the relative orientation between the state and the homodyne local oscillator.

The simulations include several internal consistency checks. First, the normalized state $aS(r)|0\rangle$ is verified to coincide with $S(r)|1\rangle$. Second, the Wigner negativity of $S(r)|1\rangle$ is constant with squeezing parameter r , as expected from Gaussian-unitary invariance. Third, unsqueezed Fock states provide isotropic displacement-radius references, with $R_x = R_p$ and $R_{\max}/R_{\min} = 1$. Fourth, even and odd cat responses converge at larger $\langle n \rangle$, consistent with the exponential suppression of $\langle \alpha | -\alpha \rangle$. The displacement radii are extracted by linear interpolation at the first crossing of the chosen fidelity threshold. If no crossing occurs within the scanned displacement interval, the reported radius is treated as a lower bound. These checks are used to distinguish physical saturation or convergence from finite-window numerical artifacts.

IV. RESULTS

A. State landscape

Figure 1 summarizes the state families used in this work. The top row follows the experimentally motivated route from squeezed light to photon-conditioned non-Gaussian states. The squeezed vacuum $S(r)|0\rangle$ in Fig. 1(a) is the Gaussian parent resource. It is zero-displacement and anisotropic in phase space, but its Wigner function is nonnegative and therefore $\delta = 0$. Its role is not to compete as a non-Gaussian state, but to serve as the optical input from which the conditioned states are generated.

A single subtraction event produces the state shown in Fig. 1(b). As derived in Eq. (19), this state is proportional to $S(r)|1\rangle$ in the ideal weak-tap limit. It has odd parity and therefore a negative Wigner value at the origin, consistent with Eq. (6). The one-click state is therefore the most direct photon-conditioned representative of the squeezed-Fock ladder.

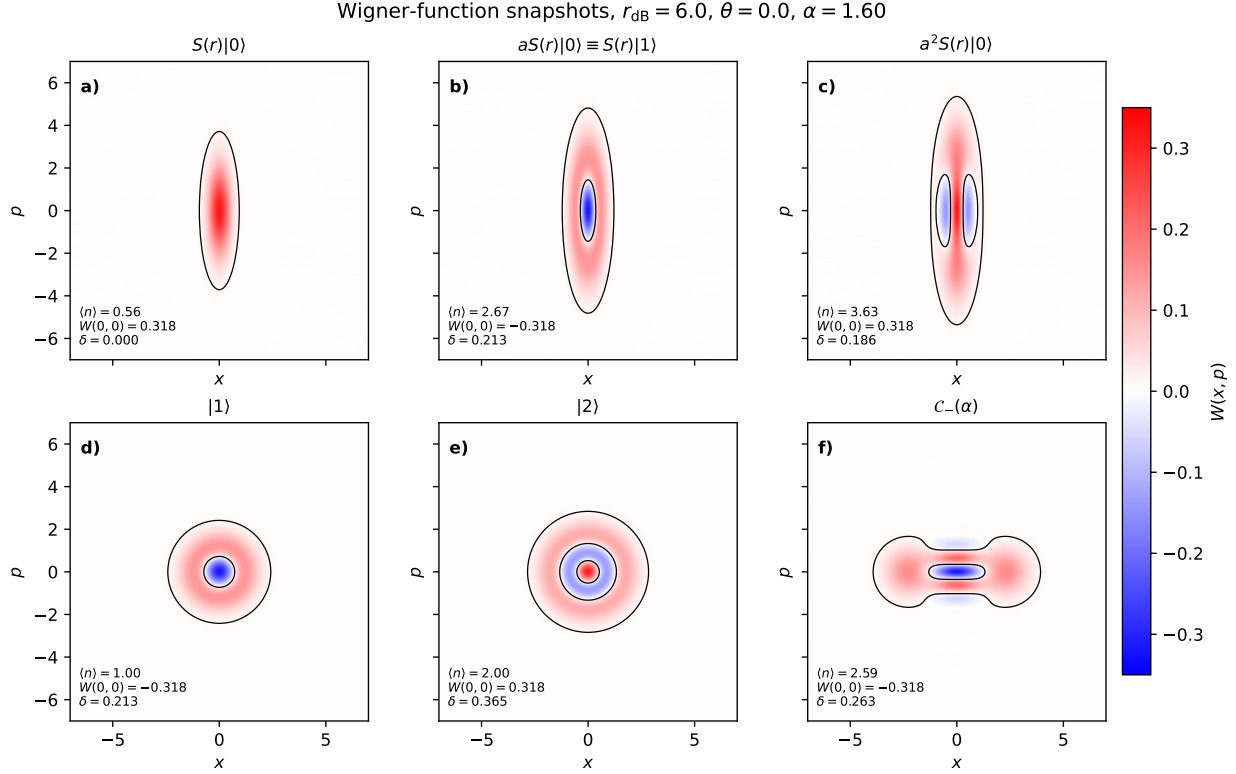


FIG. 1. Wigner-function snapshots of the state families used in the matched-energy resource comparison. The top row follows the photon-conditioning route: (a) squeezed vacuum $S(r)|0\rangle$, the Gaussian parent state; (b) the one-photon-subtracted state $aS(r)|0\rangle$, which is proportional to $S(r)|1\rangle$ in the ideal limit; and (c) the two-photon-subtracted state $a^2S(r)|0\rangle$, an even-parity squeezed Fock superposition. The bottom row shows canonical non-Gaussian references: (d) the odd Fock state $|1\rangle$; (e) the even Fock state $|2\rangle$; and (f) an odd coherent cat state $\text{Cat}_-(\alpha) \propto |\alpha\rangle - |-\alpha\rangle$. For the representative panels shown here, the squeezed-state snapshots use $r_{dB} = 6.0$ with $\theta = 0$, and the odd-cat benchmark uses $\alpha = 1.6$. All panels use the $[x, p] = i$ convention, a common phase-space window, and the same Wigner color scale. The annotated values report the mean photon number $\langle n \rangle$, the parity diagnostic $W(0,0)$, and the integrated Wigner negativity δ .

The two-click state in Fig. 1(c) shows the next member of the photon-conditioned sequence. Equation (20) shows that this state is not simply $S(r)|2\rangle$, but a squeezed superposition of $|0\rangle$ and $|2\rangle$. It has even parity and a positive central Wigner value while retaining non-Gaussian structure away from the origin. This panel is therefore important for distinguishing the ideal squeezed-Fock basis from the states produced by direct multi-photon

subtraction.

The bottom row provides reference states. The Fock states $|1\rangle$ and $|2\rangle$ isolate the odd- and even-parity Wigner structures before squeezing redistributes them in phase space. The odd cat state provides a displaced non-Gaussian benchmark. Overall, photon subtraction converts a Gaussian squeezed parent into zero-displacement, parity-resolved non-Gaussian states.

B. Matched-energy scalar resource metrics

Figure 2 shows the scalar resource metrics at matched mean photon number. For each point, r or α is chosen so that the state has the specified target $\langle n \rangle$. This removes a major ambiguity in visual Wigner-function comparisons: larger phase-space extent does not necessarily imply more non-Gaussianity per photon.

Figure 2(a) shows that the squeezed single-photon state does not gain additional integrated negativity as its mean photon number is increased by squeezing. This is expected: $S(r)|1\rangle$ is related to $|1\rangle$ by a Gaussian unitary, so the total Wigner negativity is preserved. The behavior of $a^2S(r)|0\rangle$ is different because its normalized state in the squeezed frame changes with r . At large squeezing it approaches the limiting even superposition described by Eq. (22), rather than a pure $S(r)|2\rangle$ state.

Figure 2(b) reports the energy-normalized quantity $\delta/\langle n \rangle$. This panel emphasizes that extra squeezing increases photon number without necessarily increasing total integrated negativity. Cat-state benchmarks remain strong in scalar negativity metrics because the coherent separation controls the interference structure that generates Wigner negativity. Thus, the photon-conditioned squeezed states should not be interpreted as universally superior scalar non-Gaussian resources. Their advantage, if present for a given task, must come from a different property. This conclusion is useful because it prevents an overinterpretation of the squeezed-Fock route. Photon conditioning does not provide a universal increase in scalar Wigner negativity per photon. Instead, it provides an experimentally natural, origin-centered way to introduce parity-resolved non-Gaussianity into a squeezed optical mode. The question is therefore whether this state structure is advantageous for a task whose figure of merit is not simply the total negative Wigner volume.

Figure 2(c) shows the matched parameter cost. It translates the equal-energy compar-

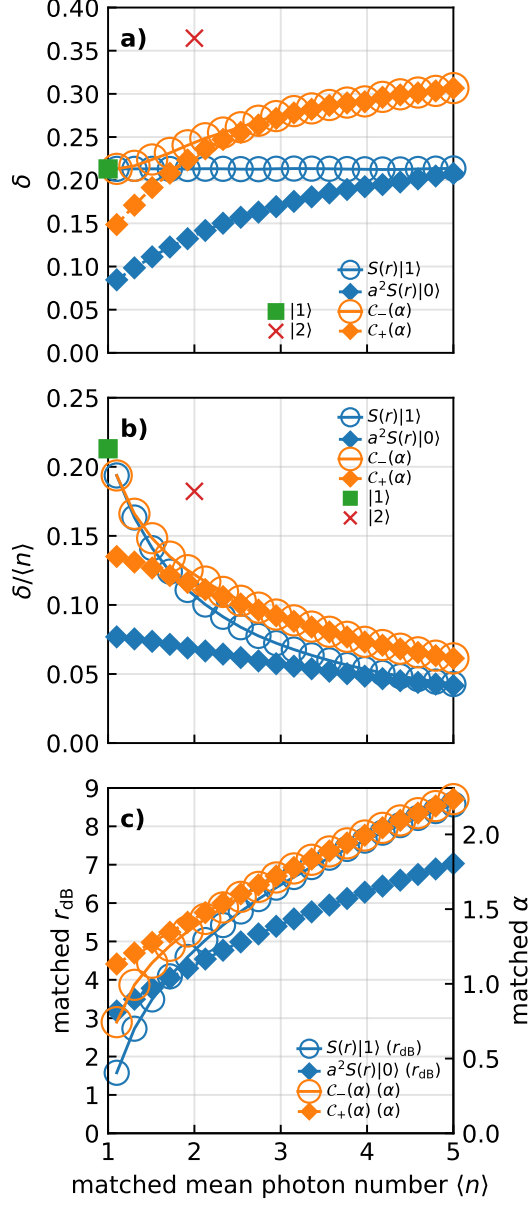


FIG. 2. Matched- $\langle n \rangle$ scalar resource metrics. (a) Integrated Wigner negativity δ versus matched mean photon number. The Fock states $|1\rangle$ and $|2\rangle$ are included as marker-only references. (b) Energy-normalized negativity $\delta/\langle n \rangle$. (c) Matched parameter cost: squeezing r_{dB} for the photon-conditioned squeezed families and cat amplitude α for the cat benchmarks.

ison into experiment: squeezing for the photon-conditioned squeezed states and coherent amplitude for the cat benchmarks. This panel is not itself a resource metric, but it makes the comparison operational.

C. Directional displacement-fidelity radii

We next evaluate directional displacement response using the same matched- $\langle n \rangle$ states. Figure 3 shows R_x , R_p , and the anisotropy ratio R_{\max}/R_{\min} at a fixed fidelity threshold. Larger R means the state remains close to itself under a larger coherent displacement in that direction.

The displacement-radius comparison reveals a tradeoff that is not visible in the scalar negativity metrics. Along one quadrature, photon-conditioned squeezed states can exhibit a substantially larger radius than the Fock and cat references over the matched-energy range shown. Along the orthogonal quadrature they can be more sensitive. The two-photon-subtracted state $a^2 S(r) |0\rangle$ is especially anisotropic: it can have the largest favorable-axis radius while also having the largest R_{\max}/R_{\min} . This should not be interpreted as a uniform advantage over cat benchmarks: the same state is less robust along the orthogonal quadrature. Its advantage is directional and therefore task dependent.

This behavior is the expected signature of squeezing. Since ideal squeezing does not increase integrated Wigner negativity, its effect appears instead as a redistribution of displacement response between conjugate quadratures. The squeezed-state advantage is therefore directional rather than universal. It is useful when the dominant displacement noise is anisotropic or can be aligned with the favorable quadrature by phase control. In this sense, Fig. 3 provides the operational counterpart to Fig. 2. The scalar metrics show how much Wigner negativity is present at a fixed photon budget, while the radius metrics show where that non-Gaussian structure is tolerant or sensitive to coherent shifts. The relevant resource is therefore not simply a larger δ , but the ability to orient the displacement response relative to a known noise direction or homodyne measurement axis. The representative polar contour in Appendix A confirms that this is not a single-axis artifact: the favorable response of the two-photon-subtracted squeezed state extends over a finite angular sector around the stretched quadrature. The axis-specific radii in Fig. 3 should therefore be interpreted as cuts through a full directional response surface $R_F(\phi)$. The cat benchmarks show a different angular mechanism. For real α , the cat components are separated along one phase-space direction. At larger matched $\langle n \rangle$, the overlap $\langle \alpha | -\alpha \rangle$ becomes small, and the even and odd cat displacement responses become nearly identical. This convergence provides an additional sanity check on the simulation and emphasizes that both cat states and squeezed-Fock re-

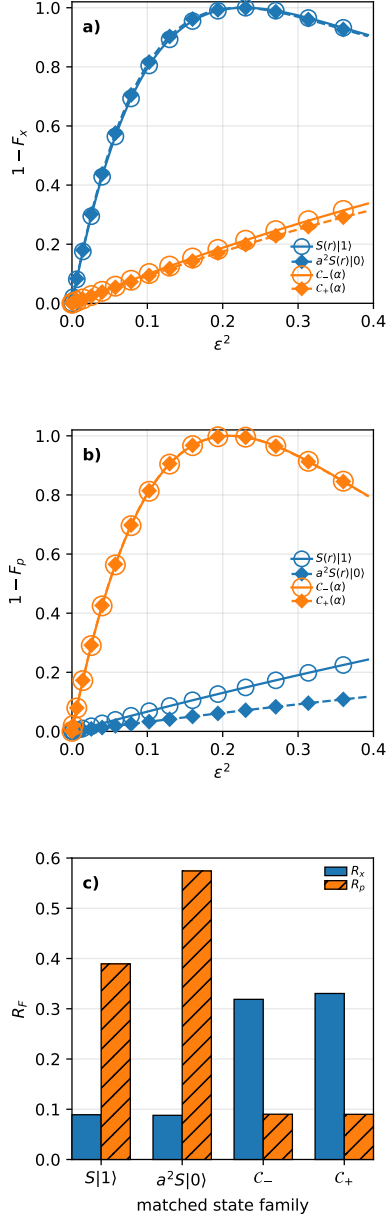


FIG. 3. Matched- $\langle n \rangle$ displacement-fidelity radii. (a) Radius R_x for displacements along the x quadrature. (b) Radius R_p for displacements along the p quadrature. (c) Anisotropy ratio R_{\max}/R_{\min} . Fock states are included as isotropic marker-only references, for which $R_x = R_p$ and $R_{\max}/R_{\min} = 1$. The radius is a fidelity-threshold diagnostic, not a full quantum-error-correction distance.

sources can be angularly tunable, but by different physical mechanisms: coherent separation for cats and squeezing axis control for photon-conditioned squeezed states.

V. DISCUSSION

A. Homodyne-aligned displacement-noise mitigation

The main application suggested by these results is homodyne-aligned anisotropic displacement-noise mitigation. Homodyne detection is a standard phase-sensitive measurement in CV photonics and is central to both optical non-Gaussian state characterization and measurement-based CV protocols [20, 21].

In a phase-referenced CV optical system, a local oscillator defines the measured quadrature. If the dominant displacement noise is known or can be aligned relative to this quadrature, then the relevant resource metric is not an angle-averaged scalar non-Gaussianity, but the displacement-fidelity radius in the noise direction.

This is the regime where photon-conditioned squeezed states can be useful despite not universally maximizing δ or $\delta/\langle n \rangle$. Their robust axis is controlled by the squeezing phase and remains centered at the origin. Cat states also have a directional response, but their anisotropy is tied to coherent-state separation. Thus the comparison distinguishes two mechanisms of angular response rather than identifying a unique capability of either family.

The same anisotropy has a dual interpretation for sensing. Along the large-radius axis, a state is robust against displacement noise. Along the small-radius axis, the local slope

$$\Gamma(\phi) = \left. \frac{d}{d\epsilon^2} [1 - F_\psi(\epsilon e^{i\phi})] \right|_{\epsilon=0} \quad (31)$$

is large, which indicates strong sensitivity to weak displacements in that direction with expected applications to sensing.

B. Relation to known state families and recent code proposals

The state families studied here are established. Squeezed number states and displaced squeezed number states have long been analyzed, including inner products relevant to displacement overlaps [6–8]. Photon-subtracted squeezed states and optical cat states have also been studied both theoretically and experimentally [9–15]. Recent measurement-based protocols further address the generation of squeezed Fock states from Gaussian resources with photon-number conditioning [16].

Squeezed-Fock states have recently been considered as bosonic-code resources and compared with squeezed-cat codewords for particle-loss and dephasing channels [17, 18]. Related conditionally squeezed oscillator states have been proposed in qubit-oscillator platforms with applications to error mitigation [22]. These works address generation protocols, encoded codewords, and channel-specific recovery or error-mitigation performance.

Our comparison is positioned differently. We do not define logical codewords, optimize a recovery map, or propose a new generation scheme. Instead, we use matched mean photon number to compare photon-conditioned squeezed states, Fock references, and cat benchmarks at the state level. The comparison separates scalar Wigner negativity from directional displacement-fidelity response, which is the metric relevant to homodyne-aligned displacement-noise geometry. This distinction matters because different tasks favor different resources: cat states can be strong scalar Wigner-negativity resources; Fock states provide isotropic displacement-response references; and photon-conditioned squeezed states provide origin-centered non-Gaussian resources whose directional response is set by the squeeze axis.

C. Resource tradeoff

The comparison suggests a simple division of roles. Cat states are strong benchmarks for scalar Wigner negativity and coherent-superposition interference. Fock states provide isotropic non-Gaussian references with no preferred displacement direction. Photon-conditioned squeezed states occupy a different regime: they are origin-centered, parity-resolved, and anisotropic. They need not maximize δ or $\delta/\langle n \rangle$ in order to be useful; their relevant advantage appears when the task has a preferred phase-space direction.

This tradeoff can be summarized as follows. If the task rewards total negative Wigner volume at fixed photon number, cat benchmarks are natural competitors. If the task requires an isotropic displacement response, Fock states provide the clean reference. If the task has a known quadrature geometry, photon-conditioned squeezed states offer a tunable response: the squeeze phase can align either the robust axis or the sensitive axis with the experimentally relevant direction. This is the regime targeted by the present work.

D. Limitations and outlook

This work does not include optical loss, finite detector efficiency, mode mismatch, or finite heralding probability. These effects are essential for a complete experimental performance model of photon-subtracted squeezed states and optical cat generation [11–15]. The present analysis also does not define a recovery operation, so the displacement-fidelity radius should not be interpreted as a full error-correction distance.

More broadly, the same phase-space benchmarking strategy can serve as a diagnostic for assessing the value of state-generation targets before substantial experimental effort is invested. This may be especially useful for structured bosonic states proposed for error-correction or protected-information applications, where preparation complexity can be high and utility is not captured by photon number or squeezing alone. By comparing Wigner negativity, phase-space structure, and characteristic length scales prior to implementation, one can identify which target states are most likely to provide useful nonclassical resources and which may offer limited practical advantage despite their preparation complexity.

The connection to grid-state synthesis is left for future work. The GKP code protects against phase-space shift errors [23], and cat-state breeding provides an established route toward approximate grid states using linear optics and homodyne measurements [24]. Recent optical schemes have also shown how squeezed cat and GKP states can be prepared deterministically from photon-number resources [25]. A single squeezed-Fock or photon-conditioned squeezed state is not a grid state, because it lacks the translational comb structure required for a GKP codeword. We do not evaluate grid-state fidelity or a breeding protocol here. Nevertheless, the origin-centered, parity-resolved Hermite-Gaussian structure of photon-conditioned squeezed states may be useful as a seed in conditional grid-state generation protocols.

VI. CONCLUSION

We have analyzed photon-conditioned squeezed light as an origin-centered non-Gaussian resource for directional displacement response in continuous-variable photonics. Single-photon subtraction from squeezed vacuum prepares a state proportional to $S(r)|1\rangle$, while two-photon subtraction prepares an even squeezed Fock superposition rather than a pure

$S(r)|2\rangle$. This algebraic distinction is essential for interpreting the resource metrics.

At matched mean photon number, cat benchmarks remain strong in scalar Wigner-negativity metrics. Photon-conditioned squeezed states do not dominate δ or $\delta/\langle n\rangle$. Their advantage appears instead in directional displacement response: squeezing redistributes fidelity radii between conjugate quadratures, allowing favorable-axis robustness at the cost of orthogonal sensitivity. This tradeoff is naturally suited to homodyne-aligned CV settings in which the dominant displacement-noise direction is known or controllable.

The broader message is that non-Gaussian resources should not be ranked by a single scalar metric alone. Matched- $\langle n\rangle$ resource mapping shows that photon-conditioned squeezed states, Fock states, and cat states occupy different regions of a tradeoff space involving Wigner negativity, photon-number cost, and directional displacement response. In this tradeoff space, the value of photon-conditioned squeezed states is not universal dominance, but origin-centered non-Gaussianity with a squeeze-axis-controlled response that can be matched to anisotropic displacement-noise geometry.

ACKNOWLEDGMENTS

B.K. gratefully acknowledges support from the U.S. National Science Foundation through QCAP-Pilot, award OSI-2410813. O.P. and B.K. acknowledge support from the U.S. National Science Foundation through the QCAP-Design program, award OSI-2531569.

DATA AND CODE AVAILABILITY

The Python code used to generate the numerical results is available at https://github.com/boriskiefer/sim_squeezed_Fock. The repository contains the research code for constructing the matched-energy state families, computing Wigner negativity, evaluating displacement-fidelity radii, and reproducing the manuscript figures from the numerical workflow. Generated data and figure files are not stored in the repository and can be regenerated by running the provided code.

Appendix A: Representative angular displacement-radius contour

The main text reports axis-specific radii R_x and R_p over a range of matched mean photon numbers. To verify that these are not single-axis artifacts, Fig. 4 shows the full angular radius $R_F(\phi)$ at a representative matched value $\langle n \rangle \simeq 3$. This value lies near the middle of the range used in Figs. 2 and 3.

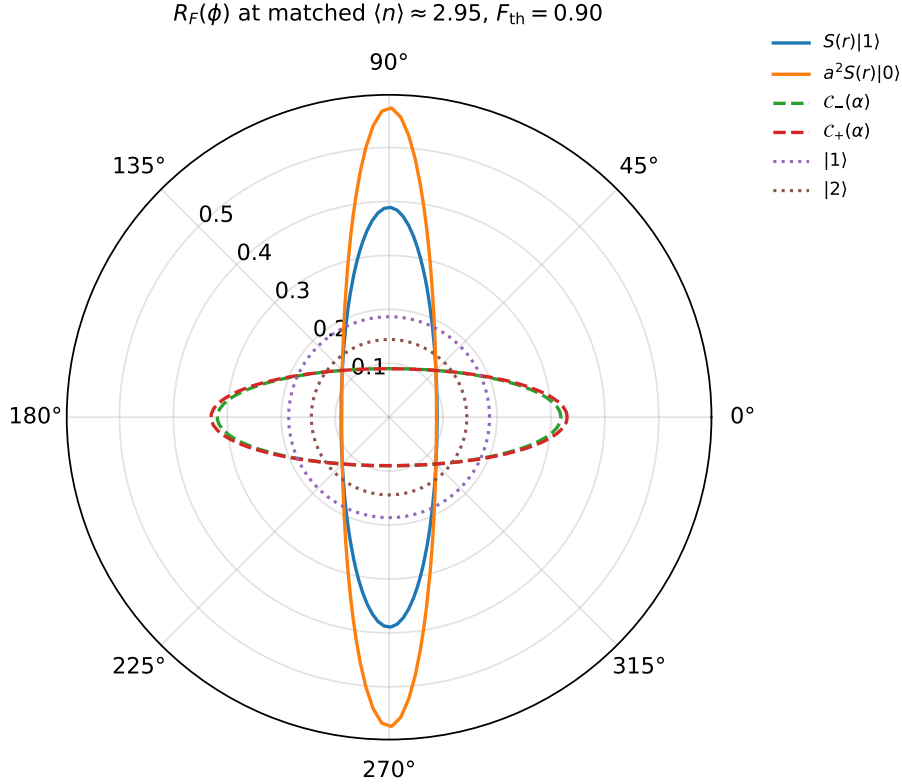


FIG. 4. Angular displacement-fidelity radius $R_F(\phi)$ at matched $\langle n \rangle \simeq 3$. The Fock-state references are isotropic, while cat and photon-conditioned squeezed states show anisotropic displacement response. The two-photon-subtracted squeezed state displays an enlarged favorable-axis radius over a finite angular sector, whereas the even and odd cat contours are nearly identical at this energy because $\langle \alpha | -\alpha \rangle$ is already small.

The polar contour also provides an angular-sector interpretation. For a chosen reference state $|\psi_{\text{ref}}\rangle$, one can define

$$\Omega_{\text{adv}} = \{\phi : R_{\text{test}}(\phi) > R_{\text{ref}}(\phi)\}. \quad (\text{A1})$$

The angular measure of Ω_{adv} identifies directions of displacement noise for which the tested

state provides a larger fidelity-threshold radius than the reference.

For comparisons with cat benchmarks, one may also define a tolerance-based sector,

$$\Omega_\eta = \{\phi : R_{\text{test}}(\phi) \geq \eta R_{\text{cat}}(\phi)\}, \quad (\text{A2})$$

with $0 < \eta < 1$. This identifies angular directions over which a photon-conditioned squeezed state is comparable to a cat benchmark rather than strictly larger. This sector-based view is the natural extension of the axis-specific radii reported in the main text.

-
- [1] S. D. Bartlett, B. C. Sanders, S. L. Braunstein, and K. Nemoto, *Phys. Rev. Lett.* **88**, 097904 (2002).
 - [2] A. Kenfack and K. Yczkowski, *J. Opt. B Quantum Semiclassical Opt.* **6**, 396 (2004).
 - [3] A. Mari and J. Eisert, *Phys. Rev. Lett.* **109**, 230503 (2012).
 - [4] V. Veitch, C. Ferrie, D. Gross, and J. Emerson, *New J. Phys.* **14**, 113011 (2012).
 - [5] M. Walschaers, *PRX quantum* **2** (2021).
 - [6] M. S. Kim, de Oliveira FA, and P. L. Knight, *Phys. Rev. A Gen. Phys.* **40**, 2494 (1989).
 - [7] K. B. Moller, T. G. Jorgensen, and J. P. Dahl, *Phys. Rev. A* **54**, 5378 (1996).
 - [8] M. M. Nieto, *Phys. Lett. A* **229**, 135 (1997).
 - [9] S. Olivares and M. G. A. Paris, *J. Opt. B Quantum Semiclassical Opt.* **7**, S616 (2005).
 - [10] A. Biswas and G. S. Agarwal, *Phys. Rev. A* **75** (2007).
 - [11] A. Ourjoumtsev, R. Tualle-Brouri, J. Laurat, and P. Grangier, *Science* **312**, 83 (2006).
 - [12] J. S. Neergaard-Nielsen, B. M. Nielsen, C. Hettich, K. Mølmer, and E. S. Polzik, *Phys. Rev. Lett.* **97**, 083604 (2006).
 - [13] K. Wakui, H. Takahashi, A. Furusawa, and M. Sasaki, *Opt. Express* **15**, 3568 (2007).
 - [14] T. Gerrits, S. Glancy, T. S. Clement, B. Calkins, A. E. Lita, A. J. Miller, A. L. Migdall, S. W. Nam, R. P. Mirin, and E. Knill, *arXiv [quant-ph]* (2010).
 - [15] K. Takase, J.-I. Yoshikawa, W. Asavanant, M. Endo, and A. Furusawa, *Phys. Rev. A* **103** (2021).
 - [16] S. B. Korolev, E. N. Bashmakova, A. K. Tagantsev, and T. Y. Golubeva, *arXiv [quant-ph]* (2023).

- [17] E. N. Bashmakova, S. B. Korolev, E. R. Zinatullin, Y. M. Golubev, and T. Y. Golubeva, J. Opt. Technol. **92**, 195 (2025).
- [18] E. N. Bashmakova, S. B. Korolev, and T. Y. Golubeva, Phys. Rev. A **112** (2025).
- [19] M. K. Hope, J. Lidal, and F. Massel, arXiv [quant-ph] (2025).
- [20] F. Lenzini, J. Janousek, O. Thearle, M. Villa, B. Haylock, S. Kasture, L. Cui, H.-P. Phan, D. V. Dao, H. Yonezawa, P. K. Lam, E. H. Huntington, and M. Lobino, Sci. Adv. **4**, eaat9331 (2018).
- [21] M. Eaton, C. Gonzalez-Arciniegas, R. N. Alexander, N. C. Menicucci, and O. Pfister, Quantum **6**, 769 (2022).
- [22] M. K. Hope, J. Lidal, and F. Massel, Phys. Rev. Res. **8** (2026).
- [23] D. Gottesman, A. Kitaev, and J. Preskill, Phys. Rev. A **64**, 012310 (2001).
- [24] D. J. Weigand and B. M. Terhal, Phys. Rev. A **97** (2018).
- [25] M. S. Winnel, J. J. Guanzon, D. Singh, and T. C. Ralph, Phys. Rev. Lett. **132**, 230602 (2024).